Unraveling Negative Feedback Translations: Gains, Peaking, Stability, and Loop Variations

Tiancheng Zhao, *Graduate Student Member, IEEE*, and Gabriel A. Rincón-Mora, *Fellow, IEEE*

***Abstract*—This brief develops a quick, precise, and insightful method for analyzing the closed-loop frequency response, peaking, and stability of complex negative feedback systems. Loop variations are explored to simplify analysis for complex feedback loops. The proposed method improves on the state-of-the-art by emphasizing circuit intuition, reducing algebraic complexity, simplifying complex feedback loops, while preserving the accuracy of the exact solution. The result shows that the closed-loop response follows the lowest forward translation across frequencies, verified by SPICE and MATLAB simulations.**

***Index Terms*—Negative feedback, frequency response, transfer function, closed-loop response, loop gain, stability, peaking, open-loop response, poles, zeros, phase margin.**

I. Negative Feedback in Electronics

NEGATIVE feedback is commonly used to control and stabilize systems. Fig. 1 depicts a system with multiple feedback paths and internal loops. The controller and feedback are optimized for specific design requirements.

Analyzing systems with multiple loops is challenging. The existing methods often involve heavy algebra prone to errors. Effective design goes beyond solving equations as it demands the designers' insights and intuition. This brief offers a more intuitive approach, based on the classical method, to determine the closed-loop response of negative feedback systems.

This brief is structured as follows: Section II introduces the derived expression, its interpretation, and other loop parameters for a single-loop model. Section III covers loop variations in complex systems. Section IV applies the method to an inverting op-amp example. Section V compares the method to state-of-the-art approaches. Section VI concludes this brief.

II. Single-Loop Feedback Model

Fig. 2 describes a single-loop feedback system. The input signal s_I is mixed with the feedback signal s_{FB}, and their difference is the error signal s_E:

$$s_E = s_I - s_{FB} \tag{1}$$

s_E is amplified to the output s_O with a *forward gain* of A_{FW}:

$$A_{FW} \equiv \frac{s_O}{s_E} = A_F \tag{2}$$

Finally, s_{FB} is "fed back" from the output s_O via a feedback network with a *feedback gain* of β_{FB}, closing the loop:

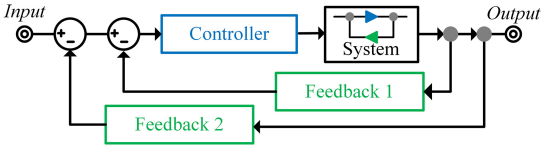

Fig. 1. Electronic system with nested feedback loops.

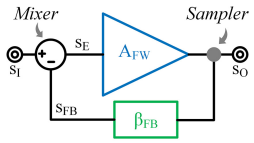

Fig. 2. Single-loop feedback model.

$$\beta_{FB} \equiv \frac{s_{FB}}{s_O} = \frac{1}{A_\beta} \tag{3}$$

The *closed-loop translation* (a.k.a. transfer function) A_{CL} of the system measures how the input signal translates to the output:

$$A_{CL} \equiv \frac{s_o}{s_I} = \frac{A_{FW}}{1 + A_{FW}\beta_{FB}} = \frac{A_{FW}\left(\frac{1}{\beta_{FB}}\right)}{A_{FW} + \frac{1}{\beta_{FB}}}$$
$$\equiv A_{FW}||\frac{1}{\beta_{FB}} = A_F||A_\beta \tag{4}$$

The first part of (4) is the classical closed-loop expression for negative feedback [1], [2], [3], [4], [5], [6], [7]. Its denominator complicates the interpretation of key information, such as poles and zeros, from complex systems where A_{FW} and β_{FB} vary with frequency. Furthermore, even after A_{CL} is rewritten to reveal its poles and zeros, its expression often looks very different from that of A_{FW} and β_{FB}, rendering any intuition gained from analyzing the two quantities less useful for design.

A. "Parallel" Closed-Loop Translation

The parallel expression at the end of (4) offers greater insights using the parallel symbol "||". Just as the lowest resistance dominates paralleled resistances, the lower of A_F and A_β governs A_{CL}. We consider both A_F and A_β as the *effective forward translations* because they represent how the input translates to the output. Thus, in Fig. 3a where the illustrative A_F (blue) and A_β (green) of a conceptual feedback system are plotted, the purple region approximates to the closed-loop gain $|A_{CL}|$. (The peak at f_{0dB3} will be explained in Section II-B.)

The poles and zeros in A_F and A_β reappear in A_{CL}, preserving the circuit intuition gained from analyzing the forward translations without rewriting the algebraic expression.

Received 6 November 2024; revised 30 December 2024; accepted 14 January 2025. Date of publication 17 January 2025; date of current version 28 February 2025. This brief was recommended by Associate Editor N. Herencsar. *(Corresponding author: Tiancheng Zhao.)*

The authors are with the School of Electrical and Computer Engineering, Georgia Institute of Technology, Atlanta, GA 30332 USA (e-mail: tzhao336@gatech.edu; rincon-mora@gatech.edu).

Digital Object Identifier 10.1109/TCSII.2025.3531242

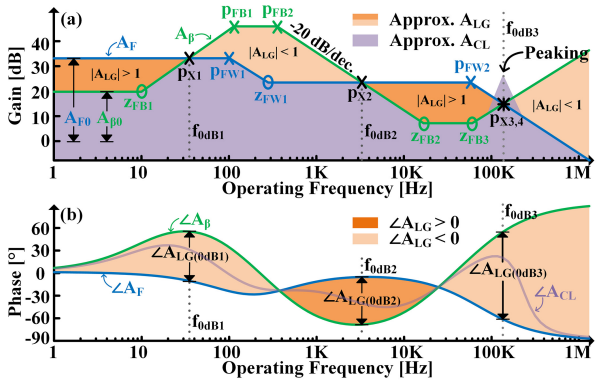

Fig. 3. Forward and closed-loop (a) gain & (b) phase response.

B. Loop Gain, Peaking, and Stability

In addition to finding A_{CL}, the loop gain A_{LG} is often used to assess the stability of the negative feedback loop across frequencies [2], [3], [6], [8], [9], [10], [11]. It is defined as the gain across the loop:

$$A_{LG} \equiv \frac{s_{FB}}{s_E} = A_{FW}\beta_{FB} = \frac{A_{FW}}{\frac{1}{\beta_{FB}}} = \frac{A_F}{A_\beta} = \frac{|A_F|\angle A_F}{|A_\beta|\angle A_\beta} = |A_{LG}|\angle A_{LG} \quad (5)$$

$|A_{LG}|$ is the logarithmic difference between $|A_F|$ and $|A_\beta|$ in dB, while $\angle A_{LG}$ is simply $\angle A_F - \angle A_\beta$. Thus, the orange regions in Fig. 3 represent the graphical quantities of $|A_{LG}|$ and $\angle A_{LG}$.

Stability can be assessed by evaluating A_{CL} at the frequency when $|A_{LG}|$ reaches unity gain (0 dB), denoted as f_{0dB}:

$$A_{CL(f_{0dB})} = \frac{A_{FW(f_{0dB})}}{1 + A_{LG(0dB)}} = \frac{A_{F(f_{0dB})}}{1 + 1\angle A_{LG(0dB)}} = \frac{A_{F(f_{0dB})}}{1 + 1\angle(PM - 180°)} \quad (6)$$

If $\angle A_{LG(0dB)} = -180°$, the system amplifies with infinite gain, causing oscillations at f_{0dB} and instability. To ensure stability, $\angle A_{LG}$ must be greater than $-180°$ at f_{0dB}, with the difference termed *phase margin (PM)*. It measures the additional phase lag or delay the system can tolerate before instability [3], [12]. A pole or a right-half plane (RHP) zero in A_{LG} reduces phase by 90°, while a left-half plane (LHP) zero increases phase by 90°.

Peaking can also be used as a hint for instability. It is defined as the fractional gain in $|A_{CL}|$ from $|A_{F/\beta}|$ at f_{0dB}:

$$|A_{CL}|_{f_{0dB}} = \left|\frac{A_{F(f_{0dB})}}{1 + A_{LG(0dB)}}\right| = \frac{|A_{F/\beta}|_{f_{0dB}}}{\sqrt{2 + 2\cos\angle A_{LG(0dB)}}} = K_p|A_\beta|_{f_{0dB}} \quad (7)$$

where $0.5 \le K_p \le \infty$. The higher the *peaking factor* K_p, the lower the PM, making the feedback loop less stable.

Multiple f_{0dB}'s can exist in a feedback system, and each must be examined to ensure stability. In Fig. 3, $\angle A_F$ and $\angle A_\beta$ are set to 0° (non-inverting) at low frequency (DC). RHP zeros are moved to higher frequencies to enhance stability. Hence, all shown poles and zeros in Fig. 3a are on the LHP. Approximations for $\angle A_{LG}$ in Fig. 3b at each f_{0dB} are as follows: at DC, $\angle A_{LG}$ is 0° as $\angle A_F$ and $\angle A_\beta$ are set equal; at f_{0dB1}, $\angle A_{LG}$ drops by less than 90° due to z_{FB1} placed half a decade before; at f_{0dB2}, A_{CL} transitions from following A_F to A_β, resulting a positive $\angle A_{LG}$; at f_{0dB3}, $\angle A_{LG}$ drops to between $-90°$ and $-180°$ due to p_{FW2} and z_{FB3} within a decade before f_{0dB3}. Peaking at f_{0dB3} is due to less than 90° of phase margin.

C. Crossings: Poles in Closed-Loop Translation

Crossings of A_F and A_β produce poles in A_{CL}. A pole in a translation drops its gain's slope by 20 dB/dec in frequency. Since $|A_{CL}|$'s slope (dB/dec) drops each time $|A_F|$ and $|A_\beta|$ overcome one another, it produces one or more equivalent poles near the crossings. In Fig. 3a, $|A_{CL}|$'s slope drops by 20 dB/dec past the crossings at f_{0dB1} and f_{0dB2}, each producing one pole p_{X1} and p_{X2}, respectively. $|A_{CL}|$'s slope drops by 40 dB/dec past f_{0dB3}, producing two poles $p_{X3,4}$. $p_{X3,4}$ is a complex conjugate pair in Fig. 3a due to peaking, indicating underdamped oscillation.

To find the exact crossing poles p_{XN} in A_{CL}, one can rewrite A_{CL} as $A_F A_\beta/(A_F + A_\beta)$ from (4), then null its denominator:

$$s|_{A_F(s)+A_\beta(s)=0} = 2\pi p_{XN} \quad (8)$$

where s is the complex operating frequency in Laplace. However, when performing steady-state frequency analyses, it is often more convenient to use $s = i2\pi f_O$, where f_O is the operating frequency (Hz). The f_{0dB}, which is only found in steady state, thus, occurs with a slightly different condition:

$$f_O|_{|A_F(i2\pi f_O)|=|A_\beta(i2\pi f_O)|} = f_{0dBN} \approx |p_{XN}| \quad (9)$$

To be precise, f_{0dB} does not always equal p_X, as it imposes no phase requirements. However, each f_{0dB} directly induces one or more p_X in A_{CL} due to the gain slope's decrease, making them closely aligned in practice, which will be shown in Section IV.

D. Frequency Response: Lowest Forward Translation

The frequency response A_X of any system can be described as:

$$A_X(s) = A_{X0}\frac{N(s)}{D(s)} = A_{X0}\left[\frac{(1 \pm s/2\pi z_1)\ldots(1 \pm s/2\pi z_N)}{(1 + s/2\pi p_1)\ldots(1 + s/2\pi p_M)}\right] \quad (10)$$

where A_{X0} is the system's DC gain, N(s) contains all the zeros, and D(s) contains all the poles. A_F and A_β in Fig. 3 are

$$A_F(s) = 45\left\{\frac{\left[1+\frac{s}{2\pi(280Hz)}\right]}{\left[1+\frac{s}{2\pi(100Hz)}\right]\left[1+\frac{s}{2\pi(58kHz)}\right]}\right\} \quad (11)$$

$$A_\beta(s) = 10\left\{\frac{\left[1+\frac{s}{2\pi(10Hz)}\right]\left[1+\frac{s}{2\pi(17kHz)}\right]\left[1+\frac{s}{2\pi(60kHz)}\right]}{\left[1+\frac{s}{2\pi(120Hz)}\right]\left[1+\frac{s}{2\pi(350Hz)}\right]}\right\} \quad (12)$$

A_{CL} can be written in the same form, with $A_{CL0} = A_{F0}||A_{\beta0}$. It has zeros at z_{FB1}, z_{FW1}, z_{FB2}, and z_{FB3} and poles at p_{X1}, p_{FW1}, p_{X2}, p_{X3}, and p_{X4}. The approximated A_{CL} can be seen as the lowest forward translation, with added peaking evaluated at the crossings in Fig. 3. It requires much less computation than the classical approach by simply applying the insights drawn from the previous discussions. The approximation is very close to the exact A_{CL} if used effectively, which will be shown in Section IV.

III. Loop Variations

This section examines four loop variations and their applications, often encountered in complex feedback systems that the single-loop feedback model does not fully capture [12].

A. Pre-Amplifier

Fig. 4 shows a feedback system where a pre-amplifier cascades with a feedback loop. The pre-amplifier can scale, shift, or convert signals of different physical quantities (e.g.,

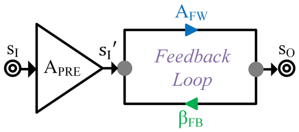

Fig. 4. Pre-amplified feedback loop.

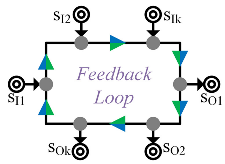

Fig. 5. Feedback loop with multiple inputs and outputs.

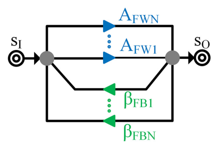

Fig. 6. Feedback loop with parallel forward and feedback paths.

current to voltage). The closed-loop translation A'_{CL} can be described as:

$$A'_{CL} = \frac{s_O}{s_I} = \left(\frac{s_I{}'}{s_I}\right)\left(\frac{s_O}{s_I{}'}\right) = A_{PRE}A_{CL}$$
$$= (A_{PRE}A_{FW})||\left(A_{PRE}\frac{1}{\beta_{FB}}\right) = A'_F||A'_\beta \qquad (13)$$

The pre-amplifier A_{PRE} effectively amplifies both A_{FW} and $1/\beta_{FB}$, making it equivalent to a single-loop feedback system with the *effective forward translations* A'_F and A'_β. All concepts in Section II can be extended to this system logically. An inverting op-amp can be analyzed using this loop variation.

B. Multiple Inputs/Outputs

A single feedback loop can mix and sample multiple input and output signals at different nodes. When the system is linear near its operating point, each output signal in Fig. 5 carries the contributions from all the loop inputs and their closed-loop translations to the output by superposition:

$$s_{OX} = \sum_{k=1}^{N} s_{Ik}A_{CLk} \qquad (14)$$

Summing amplifiers use this variation to amplify and sum all inputs using just a single feedback loop [13].

C. Parallel Paths

A feedback system can have multiple forward and feedback paths, as shown in Fig. 6. The paths with the highest gains dominate translations, where frequency response determines which paths dominate at any given frequency:

$$A'_{CL} = \sum A_{FW}||\frac{1}{\sum \beta_{FB}} = A'_F||A'_\beta \approx \max\{A_{FW}\}||\frac{1}{\max\{\beta_{FB}\}} \qquad (15)$$

In practice, one path may dominate at low frequencies, while another takes over at high frequencies. This is common for parasitic forward paths that reside within the feedback network [3], [14]. Feedforward compensation uses this variation to increase the stability and bandwidth of a feedback loop [15].

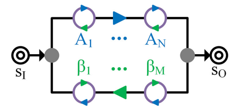

Fig. 7. Feedback loop with embedded loops.

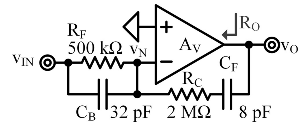

Fig. 8. Inverting op-amp circuit.

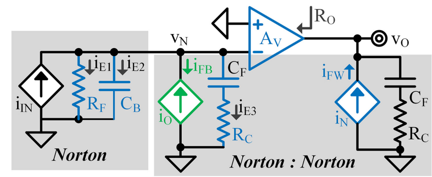

Fig. 9. Equivalent circuit of the inverting op-amp in Fig. 8.

D. Embedded Loops

Multiple inner loops can be nested inside a larger feedback loop, as shown in Fig. 7. The cascaded translations of the inner loops in the forward paths contribute to the forward translation A'_F, while those in the feedback path contribute to A'_β.

$$A'_{CL} = \left(\prod_{k=1}^{M} A_k\right)||\left(\frac{1}{\prod_{k=1}^{N} \beta_k}\right) = A'_F||A'_\beta. \qquad (16)$$

Embedded loops can be seen in almost all large systems using negative feedback, such as linear and switching regulators [12].

IV. Inverting Op-Amp Example

This section reinforces the presented concepts using an inverting op-amp circuit in Fig. 8. The op-amp's gain A_V has a DC gain A_{V0} of 100 V/V, a pole p_A at 100 kHz. This circuit is used as a type-III stabilizer in switching voltage regulators [12].

The inverting op-amp functions as a pre-amplified current-mixing loop. Fig. 9 illustrates this by applying Norton transformations of the input voltage v_{IN} with $R_F||C_B$ and the series-connected feedback network R_C and C_F [16], [17]. The pre-amplifier converts v_{IN} into an input current i_{IN}, which is mixed with the feedback current i_{FB} at node v_N. Three shunting impedances from v_N to ground translate the resulting error current i_E (i_{E1}, i_{E2}, and i_{E3}) into the voltage at v_N, which is then amplified by the op-amp to the output. The output voltage v_O is sampled and translated into i_O by the feedback network as $-i_{FB}$.

A. Forward Translations

The pre-amplifier A_{PRE} and the forward path A_{FW} are:

$$A_{PRE} = \frac{i_{IN}}{v_{IN}} = \frac{1}{R_F||\frac{1}{sC_B}} \qquad (17)$$

$$A_{FW} = \frac{v_O}{i_E} = \left(\frac{v_N}{i_E}\right)\left(\frac{v_O}{v_N}\right) = \left[R_F||\frac{1}{sC_B}||\left(\frac{1}{sC_F} + R_C\right)\right](-A_v), \qquad (18)$$

where A_v is the op-amp's gain. The effective forward translation A_{FX}, plotted in Fig. 10 in blue, can be found as:

$$A_{FX} = A_{PRE}A_{FW} = \left[\frac{\left(\frac{1}{sC_F} + R_C\right)}{\left(R_F||\frac{1}{sC_B}\right) + \left(\frac{1}{sC_F} + R_C\right)}\right]\left(\frac{-A_{V0}}{1 + \frac{s}{2\pi p_A}}\right). \qquad (19)$$

A_{FX} can also be expressed with its poles and zeros by realizing that (19) describes a voltage divider followed by

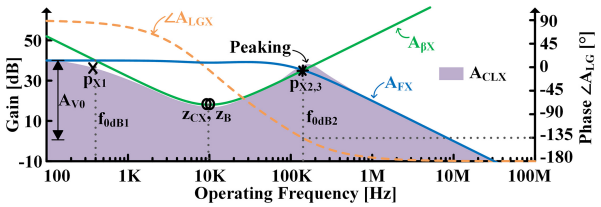

Fig. 10. Frequency response of the inverting op-amp in Fig. 8.

an amplifier ($-A_v$), which is explained in [3] as the loading effect:

$$A_{FX} \approx \left(\frac{-A_{V0}}{1+\frac{s}{2\pi p_A}}\right)\left[\frac{(1+sR_CC_F)(1+sR_FC_B)}{(1+s(R_F+R_C)C_F)(1+s(R_F||R_C)C_B)}\right]$$
$$= -\left(\frac{A_{V0}}{1+\frac{s}{2\pi p_A}}\right)\left[\frac{(1+\frac{s}{2\pi z_{CX}})(1+\frac{s}{2\pi z_B})}{(1+\frac{s}{2\pi p_C})(1+\frac{s}{2\pi p_{BX}})}\right] \quad (20)$$

where $p_C < z_{CX} = z_B < p_{BX} \ll p_A$. $A_{\beta X}$ can be found as:

$$A_{\beta X} = A_{PRE}\left(\frac{1}{\beta_{FB}}\right) = \left(\frac{i_{IN}}{v_{IN}}\right)\left(\frac{v_O}{i_{FB}}\right) = \left(\frac{1}{R_F||\frac{1}{sC_B}}\right)\left[-\left(R_C+\frac{1}{sC_F}\right)\right]$$
$$= -\frac{(1+sR_CC_F)(1+sR_FC_B)}{sR_FC_F} = -\frac{2\pi p_F\left(1+\frac{s}{2\pi z_{CX}}\right)\left(1+\frac{s}{2\pi z_B}\right)}{s} \quad (21)$$

where $p_F \ll z_{CX}, z_B$. $|A_{\beta X}|$ in (21) is plotted in Fig. 10 in green.

B. Closed-Loop Translation

The purple region in Fig. 10 shows the exact closed-loop translation A_{CLX}. A_{CLX} follows the lowest A_{FX} and $A_{\beta X}$, with poles at the crossings and zeros at z_{CX} and z_B carried from $A_{\beta X}$. To find the crossing poles, one can visually find the crossings in Fig. 10. Alternatively, we can apply (9) and solve for f_{0dB}'s. This is preferable than (8) because: 1) it is algebraically simpler to solve with a single real variable f_O, and 2) we can apply approximations to account for the effects on the gains by the poles/zeros at frequencies $f_{p/z}$ that are far from a specific f_O:

$$\left|1+\frac{s}{2\pi f_{p/z}}\right| = \sqrt{1^2+\left(\frac{f_O}{f_{p/z}}\right)^2} \approx \begin{cases} 1 & f_O \ll f_{p/z} \\ \frac{f_O}{f_{p/z}} & f_O \gg f_{p/z} \end{cases} \quad (22)$$

With the approximation, $|A_{\beta X}|$ drops below $|A_{FX}|$'s A_{V0} at the first crossing f_{0dB1} with a pole $p_F \ll p_{X1} \ll z_{CX}, z_B$:

$$|A_{FX}|_{f_O \le f_{0dB1} \approx p_{X1}} \approx A_{V0} \le \left|A_{\beta X}\right|_{f_O \le f_{0dB1} \approx p_{X1}} \approx \frac{p_F}{f_O} \quad (23)$$

Solving (23) yields $f_{0dB1} \approx |p_{X1}| = 398$ Hz, while solving with (8) yields $p_{X1} = 364$ Hz. The small difference was discussed in Section II-C. Similarly, $|A_{\beta X}|$ rises above $|A_{FX}|$ at the second crossing $f_{0dB2} \gg p_c, p_{BX}$, but close to p_A:

$$\left|A_{\beta X}\right|_{f_O \ge f_{0dB2} \approx |p_{X2,3}|} = \frac{p_F\left(1+\frac{f_O}{z_{CX}}\right)\left(1+\frac{f_O}{z_B}\right)}{f_O}$$
$$\ge |A_{FX}|_{f_O \ge f_{0dB2} \approx |p_{X2,3}|} \approx \frac{A_{V0}\left(1+\frac{f_O}{z_{CX}}\right)\left(1+\frac{f_O}{z_B}\right)}{\left(1+\frac{f_O}{p_A}\right)\left(\frac{f_O}{p_C}\right)\left(\frac{f_O}{p_{BX}}\right)} \quad (24)$$

Solving this inequality results in $f_{0dB2} \approx |p_{X2,3}| = 158$ kHz.

C. Numerical Results

Table I compares the numerical results for the exact solution, simulation, and approximations of poles and zeros in A_{CLX} and f_{0dB}'s in A_{LGX}. For the exact solution, poles are numerically found by applying (8) with MATLAB's *vpasolve*, while zeros are derived analytically from (20). For simulation, A_{CLX} is plotted, then MATLAB's *tfest* estimates its poles and zeros. f_{0dB}'s are found as the graphical crossings for the exact solution and simulation. Approximation errors occur in (23) and (24) for practical algebraic simplifications during design.

TABLE I
EXACT, SIMULATED, VERSUS APPROXIMATED SOLUTIONS

	Exact	Sim.	Approx.	Units
p_{X1}	364	364	398	Hz
z_{CX}, z_B	9.95	9.95	9.95	kHz
p_{X2}, p_{X3}	61.0 ± 153i	61.0 ± 153i	50.0 ± 150i	kHz
f_{0dB1}	399	399	398	Hz
f_{0dB2}	142	142	158	kHz

D. Stability and Peaking

Stability is evaluated using $\angle A_{LGX}$ at f_{0dB}'s in Fig. 10 (orange). At f_{0dB1}, stability is ensured as A_{CLX} transitions from A_{FX} into $A_{\beta X}$ with $\angle A_{LGX}$ of 84°. At f_{0dB2}, $\angle A_{LGX}$ is −136° (PM is 44° and K_p is 1.33), confirming stability with mild peaking.

E. Loop Variations

1) Multiple Input/Output (Summing Amplifier): Connecting the non-inverting input of the op-amp in Fig. 8 to a second voltage source v_{IN2} leads to a summing amplifier, whose output v_O can be found by superposition:

$$v_O = v_{IN}A_{CLX}|_{v_{IN2}=0} + v_{IN2}A_{CLX2}|_{v_{IN1}=0} \quad (25)$$

The forward translation A_{FX2} for this non-inverting loop is simply the op-amp's gain A_v, while $A_{\beta X2}$ can be expressed as:

$$A_{\beta X2} = \frac{1}{\beta_{FB2}} = \frac{v_o}{v_{FB}} = \frac{R_F||Z_{C_B}+R_C+Z_{C_F}}{R_F||Z_{C_B}} = 1+\frac{R_C+Z_{C_F}}{R_F||Z_{C_B}}. \quad (26)$$

Since the non-inverting and inverting op-amp share the same loop, they share the same loop gain, peaking, and stability.

2) Parallel Path (Forward-Parallel Path): Accounting for the op-amp's non-ideal output resistance R_O in Fig. 8 (with v_{IN2} now disabled) introduces a forward-parallel path A_{FP} through the feedback network. A_{FP} is in parallel with the main forward path passing through the op-amp:

$$A_{FP} = \frac{v_{O(A_V=0)}}{i_E} = \left(\frac{i_{FW}}{i_E}\right)\left(\frac{v_O}{i_{FW}}\right)_{A_V=0} = \left(\frac{v_N}{i_E}\right)\left(\frac{i_{FW}}{v_N}\right)\left(\frac{v_O}{i_{FW}}\right)_{A_V=0}$$
$$= \left[R_F||Z_{C_B}||(R_C+Z_{C_F})\right]\left(\frac{1}{R_C+Z_{C_F}}\right)\left[R_O||(R_C+Z_{C_F})\right]. \quad (27)$$

The main forward path A'_{FW} is slightly altered from (18):

$$A'_{FW} = A_{FW}\frac{R_C+Z_{C_F}}{R_O+R_C+Z_{C_F}}. \quad (28)$$

$A_{\beta X}$ remains unaffected by R_O. The resulting A'_{CLX} with R_O is:

$$A'_{CLX} = \left[A_{PRE}\left(A'_{FW}+A_{FP}\right)\right]||A_{\beta X} \equiv A'_{FX}||A_{\beta X} \quad (29)$$

A_{FP} dominates and inverts A'_{FX} and A'_{CLX} to non-inverting with an RHP zero when $|A_{FP}|$ overcomes $|A'_{FW}|$ at high frequencies, degrading stability if it is before or close to f_{0dB2}.

TABLE II
A_{CL} CALCULATIONS IN DIFFERENT APPROACHES

STATE OF THE ART	A_{CL} CALCULATION	Complexity
A_β-based [18], [19]	$\left(\frac{1}{\beta_{FB}}\right)\left(\frac{A_{LG}}{1+A_{LG}}\right) = A_\beta\left(\frac{A_{LG}}{1+A_{LG}}\right)$	Medium
RR-based [14], [20], [21]	$H_\infty \frac{T}{1+T} + H_0 \frac{1}{1+T}$	Medium
SFG-based [17]	$\frac{1}{\Delta}\sum_K P_K \Delta_K$	High
This work	$A_F \| A_\beta$	Low

V. COMPARISON WITH THE STATE OF THE ART

The proposed method extends the classical feedback concept of forward and feedback gains, offering more insights into the closed-loop frequency response and its peaking than other works. Table II summarizes alternative approaches to find A_{CL} and their relative complexity. Greater complexity increases the time needed to understand, derive equations, and design a feedback system.

Reference [18], [19] express A_{CL} by using A_β with a correction factor in terms of A_{LG}. However, this correction factor becomes difficult to track across frequencies in complex loops due to the hidden poles and zeros in the denominator, limiting its use to extreme loop gain or frequency approximations and insights into the full frequency spectrum, similar to the classical expression.

Reference [14], [20], [21] provide a different feedback model with an expression that explicitly separates the forward and direct transmission paths in a single feedback loop. To draw a valid comparison, H_∞ represents A_{CL} when $A_{LG} \to \infty$, similar to A_β. H_0 represents direct transmissions without A_{LG}, similar to A_{FP}. T, referred to as the return-ratio (RR), is different but analogous to A_{LG} in simple feedback systems [2]. The similarities become evident when evaluating the A_{CL} expression for $T \to \infty$ or 0. However, in addition to its algebraic denominator $(1 + T)$, finding T requires an extra step independent from finding H_∞ or H_0, which increases complexity. Furthermore, the feedback model does not account for loop variations in complex systems.

Reference [17] offers a systematic approach for analyzing complex feedback systems using signal flow graphs (SFG) and Mason's gain formula. The expression matches the RR-based approach for a single feedback loop with a direct transmission path present but is generalized to tackle multi-loop systems. While converting the circuit to an SFG helps understand the circuit's operations and its transmission paths, the use of the gain formula is highly algebraic as Δ is also in the form of $(1 + T)$, prone to error, and provides limited insights for feedback circuit design. Nevertheless, the systemic nature of this approach can be useful for algebraic verification of closed-loop expressions.

In this brief, the different transmission paths are absorbed into A_F and A_β as parallel paths, after which their DC gains, poles, and zeros can be reused to derive the closed-loop gain and its crossing poles. Approximations such as the "lowest forward translation" and the pole/zero effects are powerful tools for faster design and intuitive understanding of frequency response and stability. The analytical expression provides the exact closed-loop response without relying on approximations.

Reference [22] presented the parallel expression but was applied only to a specific circuit. This brief formalizes and expands the expression into a comprehensive analytical method with loop variations applicable to almost all negative feedback systems.

VI. CONCLUSION

This brief presents an analytical method for determining the closed-loop response of negative feedback systems. It simplifies the analysis with an intuitive expression based on classical feedback theory and four loop variations for complex feedback systems. The method overcomes challenges in the existing approaches, including complex algebra, extreme loop-gain approximations, and limited applicability to complex systems. It enables designers to quickly determine key gains, poles, zeros, and stability (peaking) without extensive algebra, making it highly effective for design. An inverting op-amp circuit is used to verify the method, showing strong agreement with simulations. A comparison with the state of the art is made to highlight the merits and complexity of existing approaches.

REFERENCES

[1] P. R. Gray, *Analysis and Design of Analog Integrated Circuits*. Hoboken, NJ, USA: Wiley, 2009.
[2] P. J. Hurst, "A comparison of two approaches to feedback circuit analysis," *IEEE Trans. Educ.*, vol. 35, no. 3, pp. 253–261, Aug. 1992.
[3] B. Razavi, *Design of Analog CMOS Integrated Circuits*. New York, NY, USA: McGraw-Hill, 2001.
[4] Y. Chiu, "Demystifying bilateral feedback analysis," in *Proc. IEEE 11th Int. Conf. Solid-State Integr. Circuit Technol.*, 2012, pp. 1–4.
[5] A. Ochoa, "On stability in linear feedback circuits," in *Proc. 40th Midwest Symp. Circuits Syst.*, 1998, pp. 51–55.
[6] G. W. Roberts, "Single-loop feedback parameter extraction method for stability analysis of electronic circuits," in *Proc. 53rd IEEE Int. Symp. Circuits Syst.*, 2021, pp. 1–4.
[7] O. Vityaz, "Feedback modeling using bilateral two ports," *IEEE Trans. Circuits Syst. II, Exp. Briefs*, vol. 62, no. 7, pp. 686–690, Jul. 2015.
[8] B. Behmanesh and P. Andreani, "On the calculation and simulation of loop gain in feedback circuits," *IEEE Trans. Circuits Syst. II, Exp. Briefs*, vol. 70, no. 11, pp. 4033–4037, Nov. 2023.
[9] G. W. Roberts, "Identifying A(s) and β(s) in single-loop feedback circuits using the intermediate transfer function approach," *Sensors*, vol. 22, no. 11, p. 4303, 2022.
[10] Y. Yang, D. Chen, J. Wang, Z. Li, and J. Hou, "Stability of negative feedback amplifier circuit," *Res. Explor. Lab.*, vol. 31, no. 8, pp. 23–24, 2012.
[11] A. Ochoa, "Loop gain in feedback circuits: A unified theory using driving point impedance," in *Proc. IEEE 56th Int. Midwest Symp. Circuits Syst.*, 2013, pp. 612–615.
[12] G. A. Rincón-Mora, *Gabriel Alfonso Rincón-Mora, Switched Inductor Power IC Design*. Cham, Switzerland: Springer Nat., 2022.
[13] J. S. Kim, S. Ha, H. Jeong, and J. Roh, "A high-PSRR NMOS LDO regulator with intrinsic gain-tracking ripple cancellation technique," *IEEE Trans. Circuits Syst. I, Reg. Papers*, vol. 71, no. 11, pp. 4951–4960, Nov. 2024.
[14] R. D. Middlebrook, "The general feedback theorem: A final solution for feedback systems," *IEEE Microw. Mag.*, vol. 7, no. 2, pp. 50–63, Apr. 2006.
[15] G. S. Kim, J. K. Park, G.-H. Ko, and D. Baek, "Capacitor-less low-dropout (LDO) regulator with 99.99% current efficiency using active feedforward and reverse nested miller compensations," *IEEE Access*, vol. 7, pp. 98630–98638, 2019.
[16] A. Ochoa, "A systematic approach to the analysis of general and feedback circuits and systems using signal flow graphs and driving-point impedance," *IEEE Trans. Circuits Syst. II, Analog Digital Signal Process.*, vol. 45, no. 2, pp. 187–195, Feb. 1998.
[17] J. Seungwoo, S. Ickhyun, and J. D. Cressler, "Systematic methodology for applying Mason's signal flow graph to analysis of feedback circuits," in *Proc. IEEE Int. Symp. Circuits Syst. (ISCAS)*, 2014, pp. 2421–2424.
[18] M. Neag and O. McCarthy, "An extension of the classical feedback theory to voltage and current output circuits," in *Proc. Eur. Conf. Circuit Theory Design (ECCTD)*, 1997, pp. 419–424.
[19] L. Codecasa, "Novel feedback theory of electric circuits—Part II: Loop invariants," *IEEE Trans. Circuits Syst. I, Reg. Papers*, vol. 59, no. 7, pp. 1505–1518, Jul. 2012.
[20] H. W. Bode, *Network Analysis and Feedback Amplifier Design*. New York, NY, USA: D. Van Nostrand Co., 1945.
[21] S. Rosenstark, "A simplified method of feedback amplifier analysis," *IEEE Trans. Educ.*, vol. 17, no. 4, pp. 192–198, Nov. 1974.
[22] S. Tepwimonpetkun, B. Pholpoke, and W. Wattanapanitch, "Graphical analysis and design of multistage operational amplifiers with active feedback Miller compensation," *Int. J. Circuit Theory Appl.*, vol. 44, no. 3, pp. 562–583, 2016.